Polymer 235 (2021) 124301

Contents lists available at ScienceDirect

Polymer

journal homepage: www.elsevier.com/locate/polymer

Linear and nonlinear viscoelasticity of self-associative hydrogen-bonded polymers

Wei Hong, Jiaping Lin *, Xiaohui Tian, Liquan Wang **

Shanghai Key Laboratory of Advanced Polymeric Materials, Key Laboratory for Ultrafine Materials of Ministry of Education, Frontiers Science Center for Materiobiology and Dynamic Chemistry, School of Materials Science and Engineering, East China University of Science and Technology, Shanghai, 200237, China

ARTICLE INFO

Keywords:
Viscoelasticity
Hydrogen bond
Dissipative particle dynamics

ABSTRACT

We conducted a nonequilibrium dissipative particle dynamics simulation on the linear and nonlinear viscoelastic behaviors of polymer melt associated with hydrogen bonds. The effects of the number of hydrogen bonding groups and the strength of hydrogen bonding on viscoelasticity were examined. The simulation results show that the polymers with strongly associating hydrogen bonds exhibit supramolecular networks, and their motion displays some similarities to that of polymer melts following the Reptation model. The strain hardening is due to the strain-induced stretching of polymer chains in the supramolecular networks. The number and lifetime of hydrogen bonding have a combined impact on the dynamic and linear viscoelastic behaviors of self-associative polymers. The storage moduli increase linearly with increasing the numbers of hydrogen bonding groups as the lifetime of hydrogen bonds is comparable to or larger than the relaxation time of polymer chains. In contrast, hydrogen bonding has a less pronounced influence on the dynamics and viscoelasticity as the lifetime of hydrogen bonds is minimal. The results are closely aligned with the experimental findings and provide a deep insight into the viscoelasticity of self-associative polymers via hydrogen bonds.

1. Introduction

Supramolecular polymers, which are held together with directional and reversible secondary interactions, have attracted wide attention for their distinct properties derived from the reversibility of secondary bonds [1–6]. The reversibility of secondary bonds endows them widespread applications as stimuli-sensitive, self-healing, adhesive, and shape-memory materials. The secondary interactions, including hydrogen bonding, metal-ligand, π-π stacking, ionic interactions, and solvophobic interactions, can be dynamically broken and reformed in a specific time scale [7–11]. As a result, supramolecular polymers functionalized with reversible linkers can exhibit unusual and tunable viscoelastic behaviors relative to their nonassociative counterparts.

Among all supramolecular interactions, hydrogen bonding remains a topic of most interest due to its extensive existence [12–17]. In recent years, a number of studies have revealed that hydrogen bonding has a significant impact on the viscoelasticity of supramolecular polymers [18,19]. This impact is mainly determined by the strength and content of hydrogen bonding. For instance, Lewis and coauthors prepared multiple poly(butyl acrylate) copolymers bearing different types of hydrogen bonding groups (HBGs) and examined the influence of hydrogen bonding strength on viscoelasticity [20]. They found that the copolymers with weak HBGs behave as unentangled melts and exhibit enhanced dynamic moduli with increasing the number of binding groups. In contrast, the copolymers with strong HBGs exhibit the salient feature of entangled networks.

Seiffert conducted a series of studies on the linear rheology of supramolecular polymers and concluded that the noncovalent association could result in the increase of longer relaxation time (τ_l) and storage modulus (G') on timescales longer than τ_l and the decrease in frequency-dependent power-law scaling of G' [21]. Shabbir et al. synthesized neat poly(*n*-butyl acrylate) (PnBA) and four PnBA-poly(acrylic acid) copolymers with various contents of acrylic acid groups and investigated their rheological behaviors [22]. They found that on timescales longer than reptation time, the dynamic moduli increase linearly with the number of hydrogen-bonding groups. In addition to linear viscoelasticity, associative polymers usually show rich nonlinear viscoelasticity, including strain hardening and strain softening [23–26]. Huang et al. studied the nonlinear rheological properties of poly(vinyl alcohol)/-borate hydrogels and revealed the mechanisms of strain hardening [27].

* Corresponding author.
** Corresponding author.
E-mail addresses: jlin@ecust.edu.cn (J. Lin), lq_wang@ecust.edu.cn (L. Wang).

https://doi.org/10.1016/j.polymer.2021.124301
Received 26 June 2021; Received in revised form 16 October 2021; Accepted 21 October 2021
Available online 22 October 2021

They found that strain-induced non-Gaussian stretching mainly results in the intercycle strain hardening when the Deborah number (D_e) is larger than 1.

However, the interplay of polymer dynamics, sticker dynamics, polydispersity, and dynamics of possible aggregated structures in polymer melt makes interpreting the experimental data very difficult. Moreover, multiple timescales, including the lifetime of hydrogen bonds and the relaxation time of polymer chains, are coupled to play a central role in the dynamics and viscoelasticity of supramolecular polymers [28,29]. Due to the complexation, little is known about the physical origin of enhanced viscoelasticity under the influence of hydrogen bonding. For instance, the strain hardening of storage moduli could be attributed to either the shear-induced stretching of polymer chains or the shear-induced increment in the number of elastically active chains. Hence, systematically investigating the viscoelasticity of hydrogen-bonded polymers is desired for rational design and applications.

So far, theory and simulation methods have been developed to study the mechanical and rheological properties of supramolecular polymers [30–38]. Rubinstein and Semenov have conducted a series of theoretical studies on the dynamics and viscoelasticity of associative polymers [28,33,39–41]. They found that the dynamics of associative polymers are dominated primarily by the effective lifetime of reversible junctions and the network strand size. Moreover, slip-link models coupled with reversible cross-links are established to investigate the dynamic and viscoelastic properties of associative polymers [42–44]. For instance, Mateyisi et al. employed a slip-link model to examine the effect of weak reversible cross-linkers on the relaxation modulus. They found that the associative system exhibits a delayed terminal relaxation and a much higher first plateau in the elastic modulus than the nonassociative system [44]. In addition, dissipative particle dynamics (DPD) is a valuable tool for studying the rheological behaviors of copolymers [45–47]. Ganesan and coauthors utilized a nonequilibrium oscillatory shear technique based on DPD to investigate the viscoelastic properties of gels formed by amphiphilic triblock copolymers [46]. They found that the elastic modulus increases with increasing polymer concentration and demonstrated that the results well agree with other theoretical predictions and experimental observations. Xu et al. adopted DPD to study the dynamic and mechanical properties of the associative polymer via hydrogen bond [31]. It was found that supramolecular multicompartment gels show similar stiffness to nonassociative systems but higher toughness and recovery properties than nonassociative systems.

In this work, we conducted nonequilibrium DPD simulations to investigate the linear and nonlinear rheological properties of linear polymer associated with hydrogen bonds in melted states. The effects of the number of HBGs and the strength of hydrogen bonding on viscoelasticity were examined. It was found that associative polymers with high numbers of HBGs behave like entangled networks and exhibit strain hardening at large strain amplitude. The strain hardening results from the strain-induced stretching of chains before the network breaks. Moreover, the mean number and lifetime of hydrogen bonds are coupled to affect the dynamics and linear viscoelasticity of associative polymers. We expect that this work could provide new insights into the viscoelastic behaviors of associative polymers and offer valuable information for designing advanced supramolecular materials based on hydrogen bonding.

2. Models and methods

2.1. Model and condition

We considered a coarse-grained model of self-associating polymers based on the synthesized polymers consisting of a linear polymer backbone and numbers of HBGs reported in the literature [12,20,22,48]. The dissipative particle dynamics (DPD) method developed by Hoogerbrugge and Koelman was employed for the present study (More details of the DPD method are described in section 1 of supporting information) [49,50]. In the DPD simulation, a bead-spring chain was used for the polymers. The bond was set to be rigid, with a spring constant $C = 100$ and an equilibrium bond distance $r_{eq} = 0.85$. In the standard DPD, a polymer with a soft bond ($r_{eq} = 0$) was often employed to utilize fast relaxation. However, the soft bond is allowed to expand in an unphysical way easily [51]. We, therefore, used the rigid bond to reduce the unphysical expansion of the bond.

Fig. 1 shows the DPD model of self-associating polymers. As shown, each polymer consists of a linear backbone **A** and eight side groups **B** uniformly distributed along the backbone. The backbone and each side group comprise 52 and 1 beads, respectively, and the free end block of the backbone contains one bead ($L = 1$). In half of the polymer chains (acceptor-containing polymers), some (or all) of the **B** beads were treated as acceptors (red colors); in the other half (donor-containing polymers), the same number of **B** beads represent "hydrogen" (red colors). The remainder of **B** beads in acceptor- and donor-containing polymers, denoted by blue beads, cannot form hydrogen bonds. The intrachain hydrogen bonding is excluded, and only the interchain hydrogen bonding exists.

The acceptor-hydrogen-donor (AHD) 3-body interactions, which have the same functional form as DREIDING force field, describes the hydrogen bonds between side groups **B** [52]

$$U^{hb}(r_{AD}) = \begin{cases} k_A\left(20{r_{AD}}^{-12} - 24{r_{AD}}^{-10}\right)\cos^4\theta_{AHD} & \text{for } r_{AD} < R_c \text{ and } \theta_{AHD} > \theta_c \\ 0 & \text{or else} \end{cases} \tag{1}$$

where $R_c = 2.5r_c$ is the cutoff distance. θ_c and k_A are the cutoff angle and force constant, respectively, which can be adjusted to simulate the systems with different strengths and directions of hydrogen bonding. Unless specified otherwise, the k_A and θ_c are $5.0k_BT$ and 150°, respectively. r_{AD} is the radial distance between acceptor and donor, and θ_{AHD} represents the angle among the acceptor, hydrogen, and acceptor beads. Only when r_{AD} is smaller than R_c and θ_{AHD} is larger than θ_c, hydrogen bonds between side groups **B** in two different chains form. The repulsive parameters between the same kinds of beads were all set to be $25k_BT/{r_c}^2$, and those between different types of beads were chosen to be $30k_BT/{r_c}^2$.

2.2. Nonequilibrium simulation

Nonequilibrium simulation coupled with oscillatory shear technique, described in detail in our previous works, is employed to study the viscoelasticity of associative polymer melts [47]. The "fix deform" function in the large-scale atomic/molecular massively parallel simulator (LAMMPS) [53] is applied, which is conceptually identical to the most widely adopted Lees-Edwards boundary conditions [54]. An additional velocity is applied to the bead to introduce a shear field. The motion equations of the ith bead are given by the SLLOD algorithm [55]

$$\begin{aligned} \frac{d\mathbf{r}_i}{dt} &= \mathbf{v}_i + \mathbf{e}_x\dot{\gamma}r_{i,y} \\ m_i\frac{d\mathbf{v}_i}{dt} &= \mathbf{f}_i - m_i\mathbf{e}_x\dot{\gamma}v_{i,y} \end{aligned} \tag{2}$$

where $\mathbf{e}_x$ is the normalized vector, the subscript x represents the x-component of the vector. $\mathbf{f}_i$, $\mathbf{r}_i$, and $\mathbf{v}_i$ are the force, position, and velocity of ith bead, respectively. The shear rate $\dot{\gamma}$ is the time derivative of shear strain γ. The stress response is monitored, which varies sinusoidally in the linear viscoelastic region, as a sinusoidal strain is applied to the simulation box. The mathematical expressions are given by

$$\gamma = \gamma_0\sin(\omega t), \sigma_{xy} = \sigma_0\sin(\omega t + \delta) \tag{3}$$

where δ is called lag angle or phase angle, and the stress can be decomposed into two components: $\gamma_0 G' sin\omega t$ and $\gamma_0 G'' cos\omega t$, where G' is the storage modulus and G'' is the loss modulus

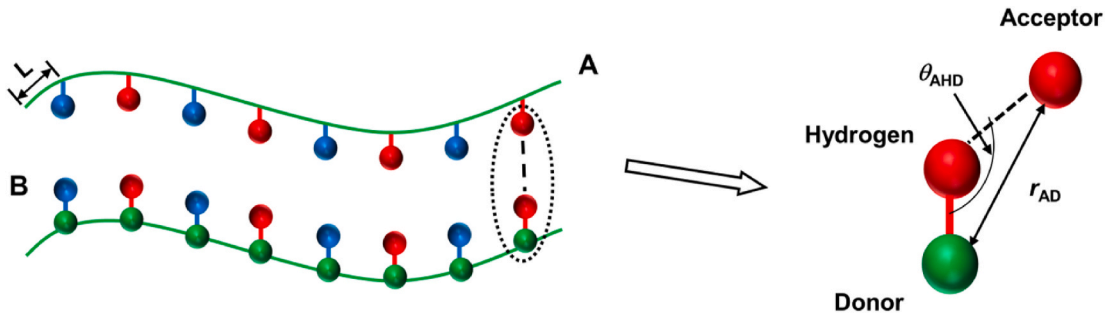

Fig. 1. DPD model of self-associating polymers constituted by a linear backbone **A** (denoted by the green line) and eight side groups **B**. For side groups, both acceptor and hydrogen are denoted by red beads, and the reminding inactive side groups are denoted by blue beads. The donors on the backbone are explicitly indicated by green beads. L denotes the length of free end blocks. Four **B** side groups are treated as hydrogen or acceptor. Each red **B** side group can form hydrogen bonds with another red **B** side group on the other chain, as shown in the enlarged view. The 3-body acceptor-hydrogen-donor potential describes the hydrogen bonding interaction, where r_{AD} is the radial distance between acceptor and donor, and θ_{AHD} represents the angle among the donor, hydrogen, and acceptor. (For interpretation of the references to color in this figure legend, the reader is referred to the Web version of this article.)

$$G' = \frac{\sigma_0}{\gamma_0}\cos(\delta), \quad G'' = \frac{\sigma_0}{\gamma_0}\sin(\delta) \tag{4}$$

The σ_{xy} can be obtained readily through the tensor version of the virial theorem

$$\boldsymbol{\sigma} = \frac{1}{V}\langle \sum_i m_i \mathbf{v}_i \mathbf{v}_i + \frac{1}{2}\sum_{i \neq j} \mathbf{r}_{ij}\mathbf{F}_{ij} \rangle \tag{5}$$

Here, V is the volume of the simulation box, $\mathbf{F}_{ij}$ is the force applied on bead j by bead i, and the angular bracket denotes an ensemble average.

The simulations were conducted in a $30 \times 30 \times 30\ r_c^3$ box with 81000 beads randomly distributed. Standard DPD simulation with periodic boundary conditions was performed by the LAMMPS [53]. The velocity-Verlet algorithm with a time step of $\Delta t = 0.01\tau$ was applied for 1×10^7 DPD steps. In the DPD simulation, we first turned off the hydrogen bonding interactions until the polymers are homogeneously mixed and then turned on the hydrogen bonding interactions for the simulation. After the system reaches equilibrium, the nonequilibrium oscillatory shear with varying amplitudes and periods was imposed. In each case, we run the nonequilibrium simulations twice to get reliable results.

3. Results and discussion

The present work focuses on the viscoelasticity of polymer melt associated with hydrogen bonds. First, we examined the nonlinear viscoelasticity of polymer melt with varied numbers of HBGs. Then we focused on the linear viscoelasticity of these self-associative polymer melts. The effects of the number of HBGs and the strength of hydrogen bonding on viscoelasticity were studied. Finally, these results were compared with existing experimental observations.

3.1. Nonlinear viscoelasticity of polymer melt associated with hydrogen bonds

Generally, supramolecular polymer networks exhibit abundant nonlinear viscoelastic properties, including strain softening and strain hardening [26]. We started with the study of nonlinear viscoelasticity of self-associative polymer melts with varying numbers (N_s) of HBGs. Fig. 2 shows the G' and G'' of polymer melts with various N_s as a function of strain amplitude under the shear frequency of $\omega = 0.01\tau^{-1}$. The G' and G'' in the nonlinear regime were obtained by fitting the stress curve with a single-harmonic sine wave [56]. The $N_s = 0$ means that there is no HBG on the backbone. The arrangement of HBG along the backbone chain with various N_s is shown in Fig. S1a. For the strength of hydrogen bonding we studied, the HBG arrangement has little impact on viscoelasticity. For example, we constructed three models for $N_s = 4$ with

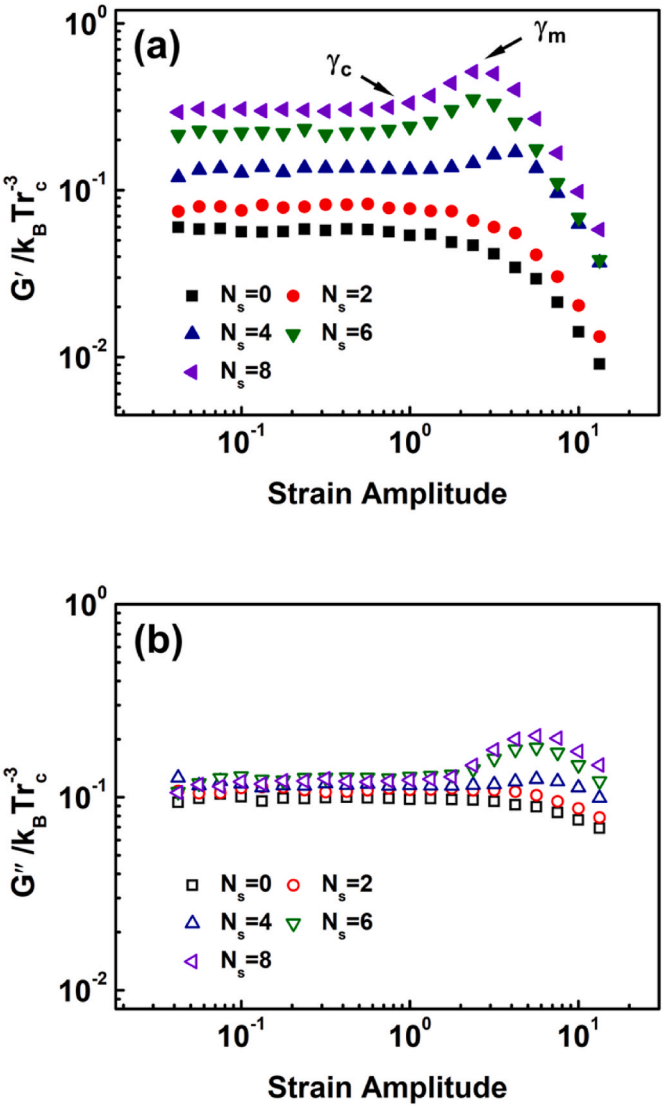

Fig. 2. (a) Storage moduli (G') and (b) loss moduli (G'') versus strain amplitude for polymer melts with varying numbers of HBGs (N_s) under the shear frequency of $\omega = 0.01\tau^{-1}$ (τ is the time unit used in DPD simulation). γ_c and γ_m represent the strain amplitudes at which strain hardening and strain softening start to appear, respectively.

multiple sequences of HBGs, including alternative, center, and two-end distributions (see Fig. S1b). Figs. S1c and d show a comparison of G' and G'' for systems with various sequences of HBGs. The G' (and G'') of the three systems are close to each other over the entire frequency range, indicating that the influence of the HBG arrangement on the viscoelasticity is minimal.

As shown in Fig. 2, the strain-independence of G' and G'' was observed in the small-strain regime for all systems. For the systems with $N_s = 0$ and 2, the G' and G'' decrease with the increase of strain in the large-strain regime, which is termed as strain softening. By contrast, strain hardening (dynamic modulus increases with increasing the strain), followed by strain softening, in the G' and G'' at large strain amplitudes was observed for the systems with $N_s = 4$, 6, and 8. The strain amplitude γ_c at the onset of strain hardening is ca. 1.77 for the system with $N_s = 4$, larger than that for the systems with $N_s = 6$ and 8 (both are ca. 1.0). In addition, the extent of increase in G' and G'' for the system with $N_s = 4$ is much smaller than that for the systems with $N_s = 6$ and 8. These results indicate that the supramolecular network can form in the systems with $N_s = 4$, 6, and 8, and the associative groups increase with increasing N_s.

So far, two possible mechanisms have been proposed to account for strain hardening in storage moduli [23,24,27]. One is the stretching of chains before the network breaks, and the other is the strain-induced increment in the number of elastically active chains. The mechanism was revealed by experimentally investigating the relaxation time of networks, the phase angle, and the degree of strain hardening [27]. Nevertheless, a molecule-level insight into the origin of strain hardening is lacked and desired. In the present work, we can reveal the mechanisms by analyzing the mean bond length ($<l_b>$) and the mean number ($<N_h>$) of hydrogen bonds, respectively. The $<N_h>$ is conceptually identical to the number of elastically active chains due to the absence of intrachain hydrogen bonding. Fig. 3 shows the $<l_b>$ and $<N_h>$ for the systems with various N_s as a function of strain amplitude. The $<l_b>$ and $<N_h>$ are calculated based on 1000 data over five oscillatory periods. As shown, both the $<l_b>$ and $<N_h>$ show strain-independence in the small-strain regime. It is interesting to find that the $<l_b>$ in systems with $N_s = 6$ and 8 starts to increase as γ is about 1. At the same strain, the strain hardening in G' starts to appear (see Fig. 2a). In addition, there is no dramatic increase in the $<N_h>$ during the strain hardening. A similar phenomenon exists in the system with $N_s = 4$. These results demonstrate that the strain-induced stretching of polymer chains in the supramolecular network contributes to the strain hardening of G'.

The $<N_h>$ for the systems with $N_s = 2$ keeps almost unchanged over the whole strain, while those for the systems with $N_s = 4$, 6, and 8 start to decrease as the strain amplitude is higher than a critical value γ_x. The critical values γ_x in Fig. 3b are consistent with the γ_m (at which storage moduli reach a maximum) in Fig. 2a, indicating that the strain softening in the supramolecular network is closely related to the mean number of hydrogen bonds. The decrease of $<N_h>$ implies the loss of associative groups. In addition, for the systems without network ($N_s = 0$ and 2), the increase of $<l_b>$ in Fig. 3a takes place as strain amplitude is ca. 1.77, which is consistent with the strain amplitude at the onset of strain softening (Fig. 2a). This implies that the increase of $<l_b>$ in systems with $N_s = 0$ and 2 are closely related to the strain softening in G'. The increased $<l_b>$ probably results from the orientation of polymers along the shear direction, implying the easy motion of polymer chains and decreased storage modulus. The number of hydrogen bonds has no apparent increase during strain hardening; the strain hardening in supramolecular networks originates from the strain-induced stretching of polymer chains. The physical origin of strain hardening is revealed on the molecular scale in the simulations.

3.2. Linear viscoelasticity of polymer melts associated with hydrogen bonds

The effect of hydrogen bond numbers on the linear viscoelasticity In this subsection, we focused on the linear viscoelasticity of associative polymer melt with various numbers of hydrogen bonds. According to Fig. 2, the strain $\gamma = 0.1$ within the linear regime was adopted in the following simulations. Fig. 4 shows the G' and G'' of associative polymer melts with various N_s versus shear frequency ω. The moduli at lower and higher frequencies are not shown because of the limitation of simulation methods. For the system without hydrogen bonding ($N_s = 0$), the terminal behavior of $G' \sim \omega^2$ at low frequencies and the relationship of $G' \sim \omega^{0.5}$ at high frequencies demonstrate that the system generally obeys the Rouse dynamics [57,58]. The frequency at which G' displays a turning point is the inverse of Rouse relaxation time. By calculating the relaxation spectra of the normal modes, we can gain the longest relaxation time (i.e., Rouse relaxation time) [58]. As shown in Fig. S2, the Rouse relaxation time has a value of 435.1τ, which is consistent with the frequency of turning point in Fig. 4a.

The systems with $N_s = 4$, 6, and 8 show rubbery-like behaviors because of the plateau in the G' ($G' \sim \omega^0$). This represents the formation of supramolecular networks. The association of hydrogen bonds results in the decline of the exponent in the power-law dependence. Additionally, it was observed that the hydrogen bonding has a striking impact on the G' but a less marked effect on the G''. The G' increases dramatically with the increase of N_s, mainly at low frequencies. In addition, a comparison between G' and G'' for various systems was made (Fig. S3). As

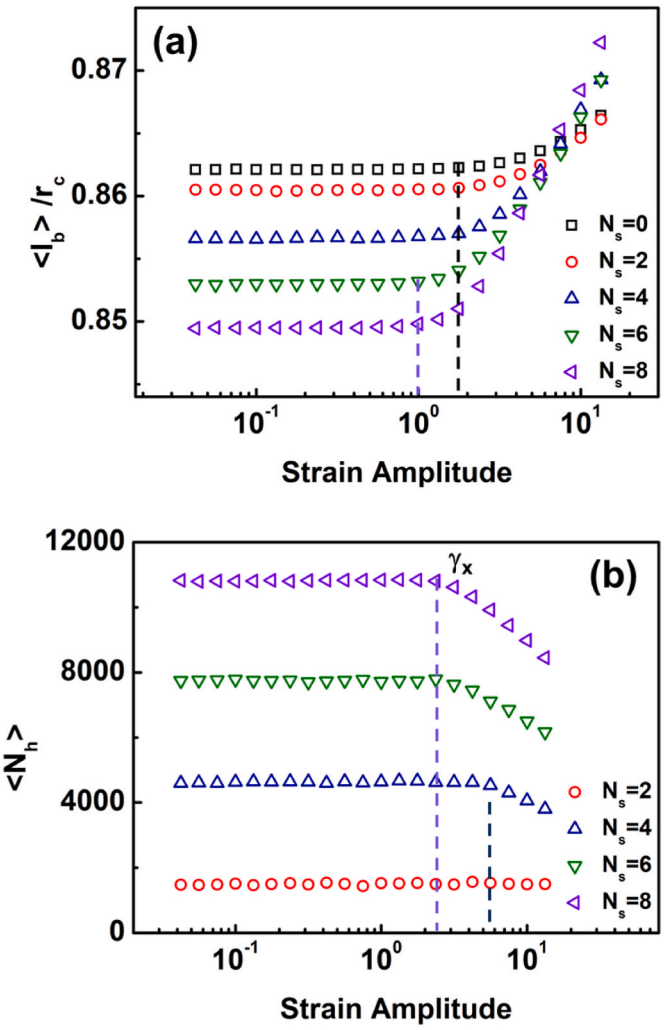

Fig. 3. (a) Mean bond length ($<l_b>$) and (b) mean number ($<N_h>$) of hydrogen bonds as a function of strain amplitude for polymer melt with varying numbers N_s of HBGs. γ_x represents the critical strain amplitude at which $<N_h>$ starts to decrease.

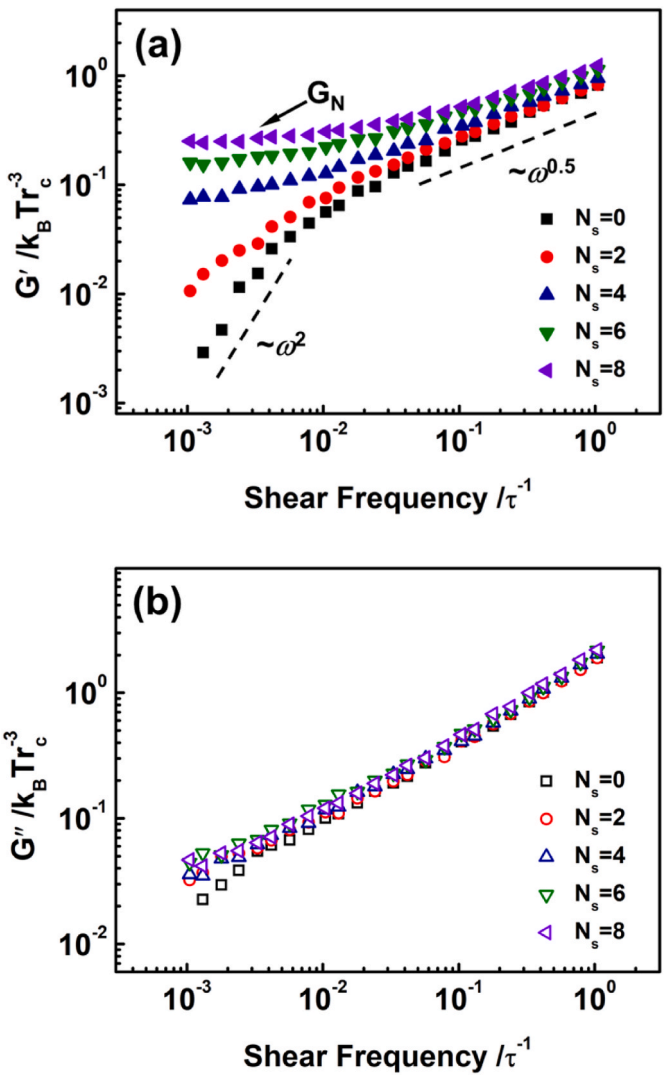

Fig. 4. (a) Storage moduli (G') and (b) loss moduli (G'') versus shear frequency for polymer melt with varying numbers N_s of HBGs. The strain amplitude is 0.1, and G_N is the plateau modulus of the network structure.

shown, for the systems with $N_s = 0$ and 2, the G'' is larger than G' over the entire frequency range, indicating liquid-like viscoelasticity. The terminal behavior was not observed for the system with $N_s = 2$ in the frequency range applied, implying that the association of HBGs increases the longest relaxation time. Meanwhile, the G' is higher than G'' at low frequencies for the systems with $N_s = 4$, 6, and 8. A crossover of G' and G'' is observed at high frequency, indicating that a solid-to-liquid transition occurs with increasing the shear frequency. According to the rubber elasticity theory, we can calculate the plateau modulus of the network structure, $G_N = nk_BT/V$, where n is the number of elastically effective strands [59]. For the system with $N_s = 8$, the $<N_h>$ in the equilibrium state is 10378.6, and therefore $G_N = 0.384k_BTr_c^{-3}$, which is consistent with the value shown in Fig. 4a.

In order to characterize the formation of percolation networks, we calculated the weight-average degree of polymerization (X_w) for systems with various N_s. The X_w is given by

$$X_w = \frac{\sum N_i^2}{\sum N_i} \tag{6}$$

where N_i is the total bead number of ith chain. Once a hydrogen bond forms between two chains, the two chains are treated as one chain. Because the periodic boundary condition was adopted in the simulation, each system contains virtually unlimited numbers of the same boxes called images. As such, we built up an expanded box containing N_{image} images and then calculated the X_w in the expanded box. X_w is independent of N_{image} if the polymer chains form discrete clusters, but X_w increases with the increase of N_{image} if percolation networks form [60]. Fig. 5a shows the dependence of X_w on N_s for polymer melts with various N_{image}. The X_w at various N_{image} increases rapidly and then keeps almost unchanged as the N_s increases. In addition, the X_w for systems with $N_s =$ 4, 6, and 8 increases dramatically with increasing N_{image}, demonstrating the percolation networks form in these systems.

To discern the role of hydrogen bonding, we calculated the mean number ($<N_h>$) of hydrogen bonds based on 1000 data for the self-associative polymer melt at an equilibrium state. Fig. 5a also shows the $<N_h>$ as a function of the HBG number N_s. We can see that the $<N_h>$ increases linearly with N_s, indicating more hydrogen bonds form in polymers with more HBG numbers. Fig. 5b shows the dependence of storage moduli G' on $<N_h>$ at fixed frequencies of $\omega = 0.1$ and 0.01. As shown, both G' at two frequencies increase linearly with $<N_h>$, demonstrating that the $<N_h>$ plays a vital role in the viscoelasticity of self-associative polymers. A similar finding was observed by Serffert [21], who explained the underlying mechanism by dividing the G' of supramolecular polymers into two parts, those are, $G'_{polymer}$ and $G'_{sticker}$. The $G'_{polymer}$ and $G'_{sticker}$ originate from the relaxation of polymer chains and sticker-related dynamics, respectively. The $G'_{polymer}$ remains unchanged for various systems, while the $G'_{sticker}$ increases linearly with the number of hydrogen bonding, resulting in the linear increase of the total storage modulus G'. Our simulation results are consistent with the experimental results.

To understand the dynamics of polymer chains, we calculated the mean square displacements (MSDs) of polymer beads (including HBGs) in the equilibrium state, as shown in Fig. 5c. The calculation details of MSD can be found in section 5 of supporting information. All the MSD curves are nearly superposed within a short-time scale with the slopes ν close to 1.0 in double logarithmic coordinates, indicating the effect of hydrogen bonding on the short-time motion of polymer beads is less pronounced. For the polymers with $N_s = 0$ and 2, the slopes ν of the MSDs approach 0.5 and 1.0 in intermediate- and long-time scales, respectively. The result demonstrates that the polymer chains obey Rouse dynamics [59]. Three regimes with the slope of 0.5, 0.25, and 0.5 were observed for the polymers with $N_s = 4$, 6, and 8, respectively, in an intermediate-time scale, similar to the MSD of polymer melts that follows the Reptation model [57,61]. The longest relaxation times (τ_R for Rouse model and τ_{rep} for Reptation Model) is inversely proportional to the diffusion coefficients, which can be evaluated by calculating the slope of the MSD in the linear region. The values of diffusion coefficients for systems with $N_s = 0$, 2, and 4 (denoted by D_0, D_2, and D_4), shown in Fig. 5c, are $4.48 \times 10^{-3}r_c^2/\tau$, $2.68 \times 10^{-3}r_c^2/\tau$, and $4.91 \times 10^{-4}r_c^2/\tau$, respectively. Note that the diffusion coefficients for $N_s = 6$ and 8 are not shown because the linear region is not achieved. Therefore, we can conclude that the longest relaxation times increase with increasing N_s (or $<N_h>$).

In addition, the MSD curves shift downward with the increase of N_s, indicating that the mobility of polymer bead is reduced due to chain association by hydrogen bonding. This behavior can be intuitively illustrated by the decrease of terminal diffusion coefficients. One can see that the diffusion coefficients decrease with increasing N_s, demonstrating that the formation of hydrogen bonds can slow down the motion of polymers. We also examined the lifetime τ_d of hydrogen bonding (the inverse of the dissociation rate constant $1/k_d$), as shown in Fig. 5d. The detailed method of calculating k_d is placed in section 6 of supporting information, and time-dependent data are shown in Fig. S4. It can be seen that the τ_d decreases with the increase of N_s, and all the τ_d are larger than the Rouse relaxation time of polymers. The reason why the hydrogen bonding for $N_s = 2$ has a longer life may be that a dissociated sticker after breaking from the hydrogen bonding always tend to

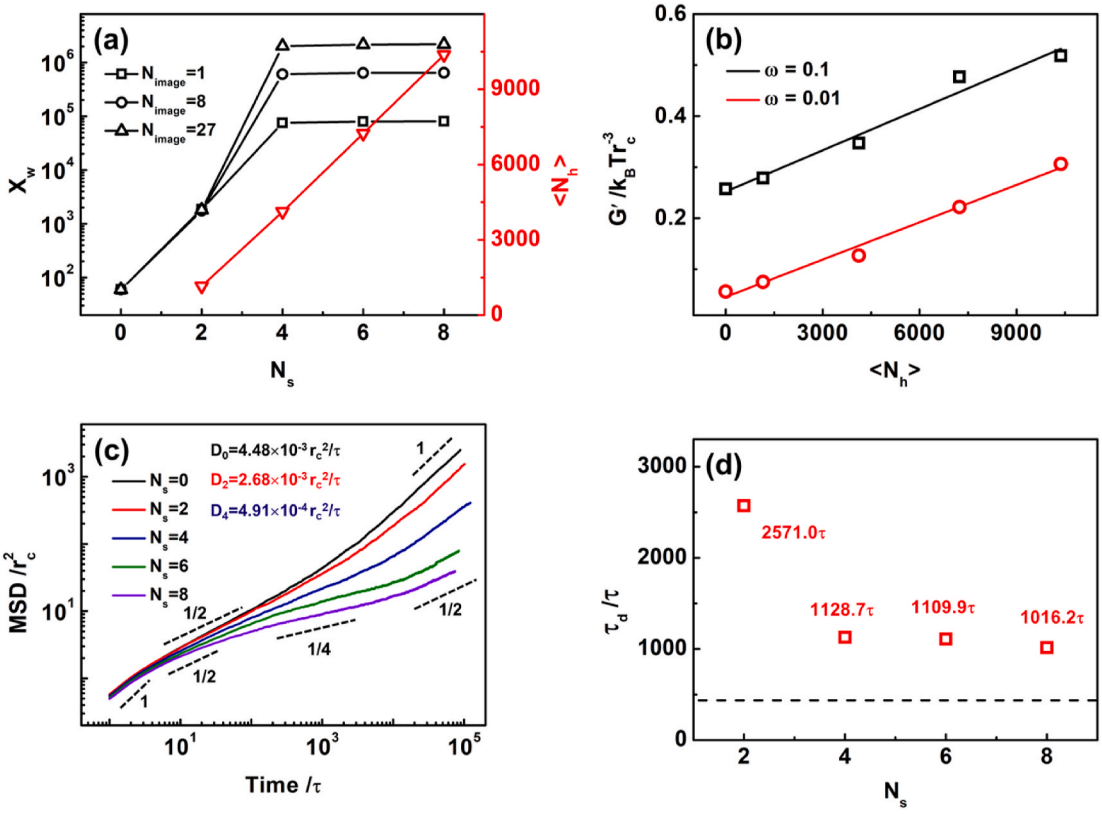

Fig. 5. (a) Weight-average degree of polymerization (X_w) calculated at various N_{image} values and mean numbers ($<N_h>$) of hydrogen bonds for polymer melts at equilibrium state as a function of N_s. (b) Storage moduli (G') at fixed $\omega = 0.1$ and $\omega = 0.01$ for polymer melt as a function of $<N_h>$. (c) Time dependence of mean-square displacements (MSDs) for polymer melt with various N_s. The diffusion coefficients are highlighted in the plot. (d) The disassociation times τ_d for polymer melts with varying N_s. The horizontal dashed line indicates the Rouse time ($\tau_R = 435.1\tau$) for a neat polymer.

associate with its old partner due to few stickers in the system, which prolongs the lifetime of hydrogen bonding [41].

3.3. The effects of the strength and directivity of hydrogen bonding on the linear viscoelasticity

In this subsection, we focused on the effect of strength and directivity of hydrogen bonding on the linear viscoelasticity of associative polymer melts. The polymer model with $N_s = 8$ is chosen for the following simulations. In terms of Eq. (1), two parameters, including force constant k_A and cutoff angle θ_c, are critical in the hydrogen bonding potential and represent the strength and direction of hydrogen bonds, respectively. Here, the two parameters are tuned to examine their influence on the linear viscoelasticity of associative polymers.

Fig. 6a shows the storage moduli G' of polymers with a varied force constant k_A versus frequency. The loss moduli G'' are shown in Fig. S5a. Note that the $k_A = 0$ suggests that the hydrogen bonding is turned off, identical to the system with $N_s = 0$. One can see that the k_A greatly influences G' but has a less marked effect on G''. For the polymer with weak hydrogen bonding ($k_A = 3$ and $4k_BT$), the G' is almost identical to that for neat polymer ($k_A = 0$) over the entire frequency range, indicating a little effect of hydrogen bonding on the storage moduli. There is a remarkable increase in G' at low frequency as k_A increases from 4 to $4.5k_BT$. For the polymers with strong hydrogen bonding ($k_A = 4.5$, 5, and $7k_BT$), there is a low-frequency plateau in G', and the plateau moduli increase with the increase of the force constant k_A. We examined the mean number $<N_h>$ of hydrogen bonding based on 1000 data for self-associative polymers with various k_A at the equilibrium state to get a deeper insight into the distinct viscoelasticity. The result is shown in Fig. 6b. For the polymers with strong hydrogen bonding ($k_A = 4.5$, 5, and $7k_BT$), the $<N_h>$ increases with k_A, resulting in the enhancement of G' according to rubber elasticity theory [59]. The associated polymers with $k_A = 3$ and $4k_BT$ exhibit quite a few hydrogen bonds ($<N_h> = 1789.4$ and 2954.5, respectively), and the hydrogen bonding has little effect on viscoelasticity. In stark contrast, the system with $N_s = 2$ has $<N_h> = 1152.0$ and show enhanced storage moduli relative to the neat polymer (see Fig. 4a).

To understand the viscoelastic behaviors of the system with $k_A = 3$, we explored the dynamics of polymer chains. Fig. 7a shows the MSDs for polymer melts with various force constants k_A. We can see that the MSDs for the polymer melts with $k_A = 0$, 3, and $4k_BT$ almost overlap, indicating little hydrogen bonding effect on polymer dynamics. The MSD curves shift downward with the increase of k_A from 4 to $7k_BT$. This can be attributed to the rise of $<N_h>$, i.e., the increase in the number density of elastically active network strands. Note that the MSD for a polymer with $k_A = 7$ exhibits a plateau at long times, which is ascribed to extreme confinement of polymer chains from highly networked structures. Fig. 7b shows the dependence of the disassociation times (lifetime) τ_d on the force constants k_A. The time-dependent data for obtaining k_d are shown in Fig. S6. The values of τ_d for the polymer with $k_A = 3$ and $4k_BT$ are 5.0 and 46.1τ, respectively, which are remarkably shorter than the Rouse time of neat polymers. The exceedingly short lifetime of hydrogen bonds shows that the motion of polymer cannot "feel" the existence of hydrogen bonding. Although there are quite a few hydrogen bonds ($<N_h> = 1789.4$) in the system, hydrogen bonds have little impact on the dynamics and viscoelasticity. The lifetime τ_d increases evidently as k_A increases from 4 to $4.5k_BT$ and then is maintained greater than the Rouse time of neat polymers. In systems with $k_A = 4.5$, 5, and $7k_BT$, the τ_d is large enough, and there are enough hydrogen bonds. As such, percolation networks can form, and a low-frequency plateau in G' appears. The above results show that as τ_d is comparable to or larger than τ_R of neat polymers, the mean number $<N_h>$ of hydrogen bonding plays

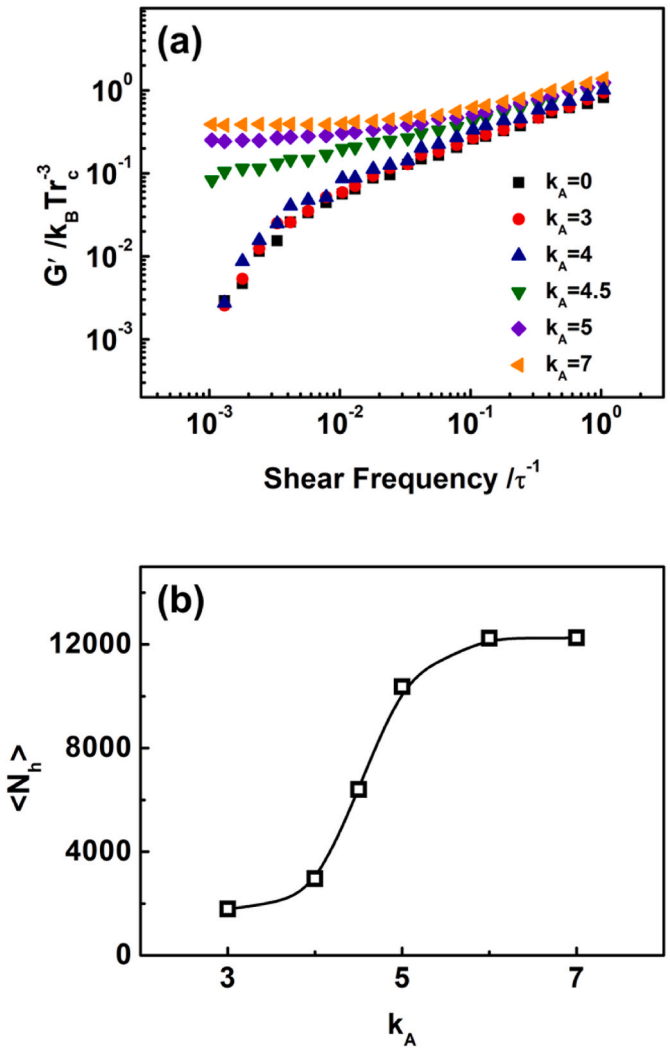

Fig. 6. (a) Storage moduli (G') versus shear frequency for polymer melt with various force constants k_A. (b) The dependency of the mean number $<N_h>$ of hydrogen bonds on the force constants k_A.

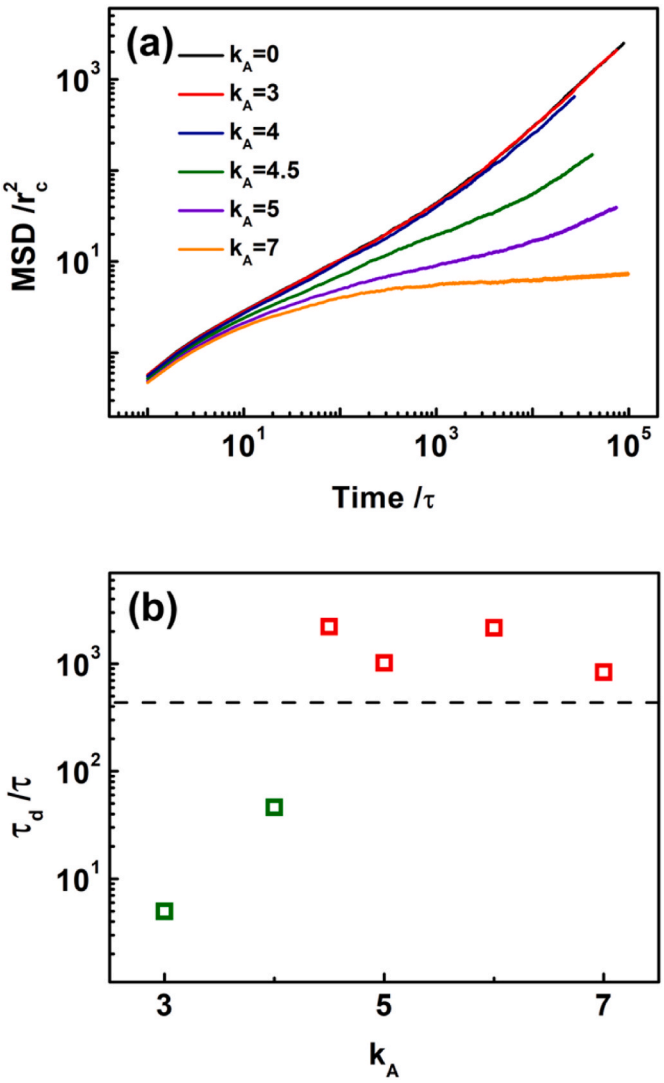

Fig. 7. (a) Time dependence of mean-square displacements (MSDs) for polymer melt with various force constants k_A. (b) The disassociation times τ_d versus the force constants k_A. The horizontal dashed line indicates the Rouse time (τ_R = 435.1τ) for a neat polymer.

a vital role in the dynamics and viscoelasticity.

Fig. 8a shows the storage moduli G' of polymers with various cutoff angles θ_c versus frequency. The loss moduli G'' are shown in Fig. S5b. One can see that the effects of cutoff angles θ_c and force constants k_A on viscoelasticity are similar. At a large cutoff angle of $\theta_c = 155°$ and 160°, the G' almost overlaps with that of neat polymers over the entire frequency range, indicating nearly no effect on the viscoelasticity. For the small cutoff angles, such as $\theta_c = 140°$, 150°, and 152.5°, there is a low-frequency plateau in G', and the plateau moduli increase with decreasing θ_c. The mean number $<N_h>$ of hydrogen bonding is also examined based on 1000 data for self-associative polymer melts with various θ_c at the equilibrium state, which is shown in Fig. 8b. The $<N_h>$ increases with the decrease of θ_c, resulting in the enhancement of G' according to rubber elasticity theory [59]. A few hydrogen bonds ($<N_h> = 1971.4$ and 767.8) are formed in self-associative polymer as $\theta_c = 155°$ and 160°. The MSDs for polymer melts with various cutoff angles θ_c are shown in Fig. 9a. Similar to the observations in Fig. 7a, the MSD curves for $\theta_c = 155°$ and 160° are almost identical to that for neat polymer, but the MSD curve for $\theta_c = 140°$ shifts downward and exhibits a long-time plateau. The dependence of the disassociation times (lifetime) τ_d on the cutoff angles θ_c is shown in Fig. 9b. The time-dependent data for obtaining k_d are shown in Fig. S7. As shown, there is a significant decline in the τ_d with increasing θ_c from 152.5° to 155°. For the systems with $\theta_c = 155°$ and 160°, the lifetimes τ_d (11.8τ and 3.8τ) are markedly below the Rouse time of neat polymers. These results prove again that the mean number $<N_h>$ of hydrogen bonding predominates the dynamics and viscoelasticity of self-associative polymers as τ_d is comparable to or larger than τ_R.

3.4. Comparison with existing experimental findings

The present work has shown that self-associative polymers with fewer HBGs show strain softening at large strain amplitude. Still, those with high HBG numbers exhibit strain hardening of both storage and loss moduli. The strain hardening in storage moduli originates from the strain-induced stretching of polymer chains. Similar results exist in the experimental observations [24–27]. For example, Huang et al. observed four types of large-amplitude oscillatory shear behavior and revealed the mechanisms of strain hardening [27]. They found that the strain-induced non-Gaussian stretching almost results in the strain hardening when $D_e > 1$. Note that the D_e in our simulations is larger than 1 because the relaxation time τ_P (much larger than 100τ) is much larger than $1/\omega_s$ (ω_s adopted in Fig. 2 is $0.01\tau^{-1}$).

We also found that the self-associative polymers with high HBG

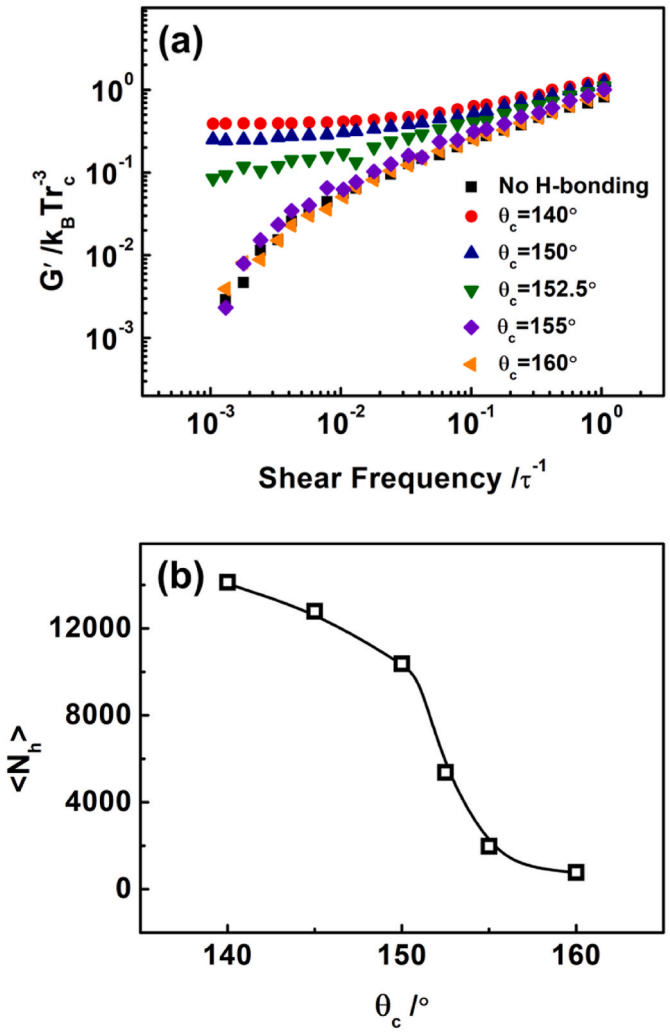

Fig. 8. (a) Storage moduli (G') versus shear frequency for polymer melt with various cutoff angles θ_c. (b) The dependency of the mean number ($<N_h>$) of hydrogen bonds on the cutoff angles θ_c.

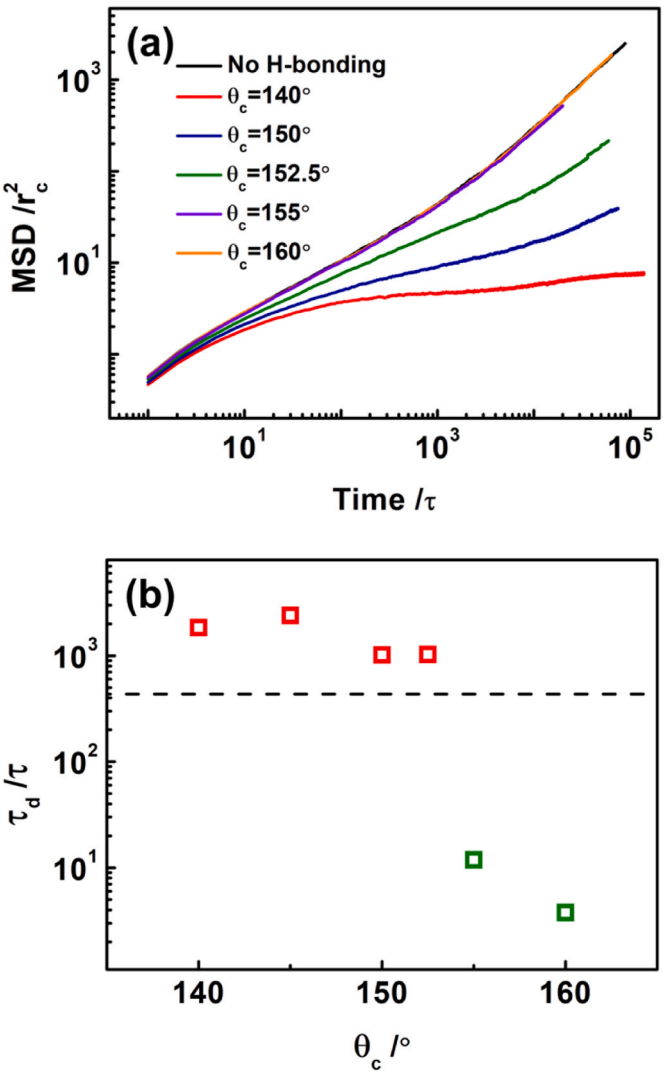

Fig. 9. (a) Time dependence of mean-square displacements (MSDs) for polymer melt with various cutoff angles θ_c. (b) The disassociation times τ_d versus the cutoff angles θ_c. The horizontal dashed line indicates the Rouse time (τ_R = 435.1τ) for a neat polymer.

numbers bear transient supramolecular networks (see Fig. 5a). The storage moduli increase linearly with the number of hydrogen bonds in linear viscoelastic regimes. Some experimental findings in the literature can support these simulation results [20–22,62,63]. For example, Lewis et al. synthesized numerous poly(*n*-butyl acrylate) (PnBA) copolymers with various numbers and types of HBG and investigated their dynamic and viscoelastic behaviors [20]. They found that the PnBA copolymers with weak and strong hydrogen bonding behave like viscoelastic liquid and entangled networks, respectively. And the storage moduli increase with increasing the number of binding groups. Shabbir et al. prepared a model system of PnBA with various numbers of acrylic acid side groups [22]. They also found that the HBGs have a pronounced influence on viscoelasticity. The storage moduli show a linear increase with increasing the number of HBGs. These experimental observations agree with our simulation results.

In addition, we found that the number and lifetime of hydrogen bonds have a combined effect on the dynamic and viscoelastic behaviors of associative polymers. And the longest relaxation time can be elevated markedly due to the existence of hydrogen bonds. The dynamics and viscoelasticity are governed by the mean number $<N_h>$ of hydrogen bonds as τ_d is comparable to or larger than τ_R. Seiffert also found that the association of secondary interactions can increase the longest relaxation time of polymers [21]. Two other effects summarized in his paper — the increase of G' and the decrease of power-law scaling of G' — can also be found in our simulation. These theoretical analyses and experimental data are in good qualitative agreement with our simulation results.

Apart from the reproduction of general characteristics of experimental observations, the simulations can help systematically examine the viscoelasticity of supramolecular polymers and reveal the physical origin on the molecular scale. Experimentally, it is difficult to control a single variable; for example, a general way to change the strength of hydrogen bonding is to change the type of HBGs, which usually leads to changes in the molecular structure. In addition, it is hard to probe into the experimental phenomena directly on the molecular scale. Therefore, some mechanisms of distinct viscoelasticity found in experiments need to consolidate from molecule-level studies; for instance, whether the strain hardening of storage moduli in the supramolecular network could originate from chain stretching or an increase in the number of elastically active chains. In the simulations, it is convenient to count the number of hydrogen bonds and obtain the data of bond lengths (see Fig. 3). By means of the DPD simulation, we can intuitively understand that the chain stretching induced by shear results in the strain hardening of supramolecular networks.

4. Conclusions

We studied the linear and nonlinear rheological behaviors of self-associative polymers through the DPD simulation coupled with a nonequilibrium oscillatory shear technique. The results show that the self-associative polymers with high numbers of HBGs exhibit strain hardening at large strain amplitude, attributed to the strain-induced stretching of polymer chains in supramolecular networks. The number and lifetime of hydrogen bonds play a vital role in the dynamic and viscoelastic behavior of self-associative polymers. The storage moduli show a linear increase with increasing the number of HBGs as the lifetime of hydrogen bonds is comparable to or larger than the relaxation time of polymer chains. However, the hydrogen bonding has a less marked effect on the dynamics and viscoelasticity as the lifetime of hydrogen bonds is remarkably lower than the Rouse relaxation time of polymers. We expect that the present work can deepen the understanding of self-associative polymer viscoelasticity and provide valuable information for designing supramolecular materials with superior properties.

CRediT authorship contribution statement

Wei Hong: Methodology, Software, Investigation, Formal analysis, Writing – original draft. **Jiaping Lin:** Conceptualization, Resources, Writing – review & editing, Funding acquisition. **Xiaohui Tian:** Validation, Supervision. **Liquan Wang:** Conceptualization, Methodology, Software, Validation, Formal analysis, Writing – review & editing.

Declaration of competing interest

The authors declare that they have no known competing financial interests or personal relationships that could have appeared to influence the work reported in this paper.

Acknowledgments

This work was supported by the National Natural Science Foundation of China (51833003, 21774032, 21975073, 22173030, and 51621002).

Appendix A. Supplementary data

Supplementary data to this article can be found online at https://doi.org/10.1016/j.polymer.2021.124301.

References

[1] G. Song, Z. Zhao, X. Peng, C. He, R.A. Weiss, H. Wang, Rheological behavior of tough PVP-in situ-PAAm hydrogels physically cross-linked by cooperative hydrogen bonding, Macromolecules 49 (2016) 8265–8273.
[2] M. Hayashi, S. Matsushima, A. Noro, Y. Matsushita, Mechanical property enhancement of ABA block copolymer-based elastomers by incorporating transient cross-links into soft middle block, Macromolecules 48 (2015) 421–431.
[3] T. Rossow, S. Seiffert, Supramolecular polymer gels with potential model-network structure, Polym. Chem. 5 (2014) 3018–3029.
[4] S. Hackelbusch, T. Rossow, P. van Assenbergh, S. Seiffert, Chain dynamics in supramolecular polymer networks, Macromolecules 46 (2013) 6273–6286.
[5] S.C. Boothroyd, D.M. Hoyle, T.C.B. McLeish, E. Munch, R. Schach, A.J. Smith, R. L. Thompson, Association and relaxation of supra-macromolecular polymers, Soft Matter 15 (2019) 5296–5307.
[6] L. Voorhaar, R. Hoogenboom, Supramolecular polymer networks: hydrogels and bulk materials, Chem. Soc. Rev. 45 (2016) 4013–4031.
[7] B.J. Gold, C.H. Hövelmann, N. Lühmann, W. Pyckhout-Hintzen, A. Wischnewski, D. Richter, The microscopic origin of the rheology in supramolecular entangled polymer networks, J. Rheol. 61 (2017) 1211–1226.
[8] H. Goldansaz, C.-A. Fustin, M. Wübbenhorst, E. van Ruymbeke, How supramolecular assemblies control dynamics of associative polymers: toward a general picture, Macromolecules 49 (2016) 1890–1902.
[9] Y. Lei, T.P. Lodge, Effects of component molecular weight on the viscoelastic properties of thermoreversible supramolecular ion gels via hydrogen bonding, Soft Matter 8 (2012) 2110–2120.
[10] D.M. Loveless, S.L. Jeon, S.L. Craig, Rational control of viscoelastic properties in multicomponent associative polymer networks, Macromolecules 38 (2005) 10171–10177.
[11] S. Ge, M. Tress, K. Xing, P.F. Cao, T. Saito, A.P. Sokolov, Viscoelasticity in associating oligomers and polymers: experimental test of the bond lifetime renormalization model, Soft Matter 16 (2020) 390–401.
[12] L.G.D. Hawke, M. Ahmadi, H. Goldansaz, E. van Ruymbeke, Viscoelastic properties of linear associating poly(*n*-butyl acrylate) chains, J. Rheol. 60 (2016) 297–310.
[13] X. Callies, C. Véchambre, C. Fonteneau, S. Pensec, J.M. Chenal, L. Chazeau, L. Bouteiller, G. Ducouret, C. Creton, Linear rheology of supramolecular polymers center-functionalized with strong stickers, Macromolecules 48 (2015) 7320–7326.
[14] X. Callies, C. Fonteneau, C. Véchambre, S. Pensec, J.M. Chenal, L. Chazeau, L. Bouteiller, G. Ducouret, C. Creton, Linear rheology of bis-urea functionalized supramolecular poly(butylacrylate)s: Part I – weak stickers, Polymer 69 (2015) 233–240.
[15] J. Nochebuena, C. Cuautli, J. Ireta, Origin of cooperativity in hydrogen bonding, Phys. Chem. Chem. Phys. 19 (2017) 15256–15263.
[16] A. Shabbir, I. Javakhishvili, S. Cerveny, S. Hvilsted, A.L. Skov, O. Hassager, N. J. Alvarez, Linear viscoelastic and dielectric relaxation response of unentangled UPy-based supramolecular networks, Macromolecules 49 (2016) 3899–3910.
[17] Y. Lin, C. Xu, A. Guan, G. Wu, Tailoring the temperature-dependent viscoelastic behavior of acrylic copolymers by introducing hydrogen bonding interactions, Polymer 161 (2019) 190–196.
[18] T. Yan, K. Schröter, F. Herbst, W.H. Binder, T. Thurn-Albrecht, What controls the structure and the linear and nonlinear rheological properties of dense, dynamic supramolecular polymer networks? Macromolecules 50 (2017) 2973–2985.
[19] S. Gupta, X. Yuan, T.C. Mike Chung, M. Cakmak, R.A. Weiss, Influence of hydrogen bonding on the melt rheology of polypropylene, Polymer 107 (2016) 223–232.
[20] C.L. Lewis, K. Stewart, M. Anthamatten, The influence of hydrogen bonding side-groups on viscoelastic behavior of linear and network polymers, Macromolecules 47 (2014) 729–740.
[21] S. Seiffert, Effect of supramolecular interchain sticking on the low-frequency relaxation of transient polymer networks, Macromol. Rapid Commun. 37 (2016) 257–264.
[22] A. Shabbir, H. Goldansaz, O. Hassager, E. van Ruymbeke, N.J. Alvarez, Effect of hydrogen bonding on linear and nonlinear rheology of entangled polymer melts, Macromolecules 48 (2015) 5988–5996.
[23] L. Pellens, R. Gamez Corrales, J. Mewis, General nonlinear rheological behavior of associative polymers, J. Rheol. 48 (2004) 379–393.
[24] D. Xu, S.L. Craig, Strain hardening and strain softening of reversibly cross-linked supramolecular polymer networks, Macromolecules 44 (2011) 7478–7488.
[25] L. Martinetti, O. Carey-De La Torre, K.S. Schweizer, R.H. Ewoldt, Inferring the nonlinear mechanisms of a reversible network, Macromolecules 51 (2018) 8772–8789.
[26] A.R. Jacob, A.P. Deshpande, L. Bouteiller, Large amplitude oscillatory shear of supramolecular materials, J. Non-Newtonian Fluid Mech. 206 (2014) 40–56.
[27] G. Huang, H. Zhang, Y. Liu, H. Chang, H. Zhang, H. Song, D. Xu, T. Shi, Strain hardening behavior of poly(vinyl alcohol)/borate hydrogels, Macromolecules 50 (2017) 2124–2135.
[28] A. Semenov, M. Rubinstein, Dynamics of entangled associating polymers with large aggregates, Macromolecules 35 (2002) 4821–4837.
[29] X. Xu, F.A. Jerca, V.V. Jerca, R. Hoogenboom, Self-healing and moldable poly(2-isopropenyl-2-oxazoline) supramolecular hydrogels based on a transient metal coordination network, Macromolecules 53 (2020) 6566–6575.
[30] N. Jiang, H. Zhang, P. Tang, Y. Yang, Linear viscoelasticity of associative polymers: sticky Rouse model and the role of bridges, Macromolecules 53 (2020) 3438–3451.
[31] P. Xu, J. Lin, L. Zhang, Supramolecular multicompartment gels formed by ABC graft copolymers: high toughness and recovery properties, Phys. Chem. Chem. Phys. 20 (2018) 15995–16004.
[32] P.D. Yeh, A. Alexeev, Mesoscale modelling of environmentally responsive hydrogels: emerging applications, Chem. Commun. 51 (2015) 10083–10095.
[33] A. Semenov, J.-F. Joanny, A. Khokhlov, Associating polymers: equilibrium and linear viscoelasticity, Macromolecules 28 (1995) 1066–1075.
[34] T. Jiang, L. Wang, J. Lin, Mechanical properties of designed multicompartment gels formed by ABC graft copolymers, Langmuir 29 (2013) 12298–12306.
[35] M. Wilson, A. Rabinovitch, A.R.C. Baljon, Computational study of the structure and rheological properties of self-associating polymer networks, Macromolecules 48 (2015) 6313–6320.
[36] J. Castillo-Tejas, O. Castrejón-González, S. Carro, V. González-Coronel, J.F. J. Alvarado, O. Manero, Associative polymers. Part III: shear rheology from molecular dynamics, Colloids Surf., A 491 (2016) 37–49.
[37] N. Jiang, H. Zhang, Y. Yang, P. Tang, Molecular dynamics simulation of associative polymers: understanding linear viscoelasticity from the sticky Rouse model, J. Rheol. 65 (2021) 527–547.
[38] Y. Peng, T. Yue, S. Li, K. Gao, Y. Wang, Z. Li, X. Ye, L. Zhang, J. Liu, Rheological and structural properties of associated polymer networks studied via nonequilibrium molecular dynamics simulation, Mol. Syst. Des. Eng. 6 (2021) 461–475.
[39] M. Rubinstein, A.N. Semenov, Thermoreversible gelation in solutions of associating polymers. 2. Linear dynamics, Macromolecules 31 (1998) 1386–1397.
[40] A.N. Semenov, M. Rubinstein, Thermoreversible gelation in solutions of associative polymers. 1. Statics, Macromolecules 31 (1998) 1373–1385.
[41] M. Rubinstein, A.N. Semenov, Dynamics of entangled solutions of associating polymers, Macromolecules 34 (2001) 1058–1068.

[42] M.E. Shivokhin, T. Narita, L. Talini, A. Habicht, S. Seiffert, T. Indei, J.D. Schieber, Interplay of entanglement and association effects on the dynamics of semidilute solutions of multisticker polymer chains, J. Rheol. 61 (2017) 1231–1241.
[43] T. Indei, J.-I. Takimoto, Linear viscoelastic properties of transient networks formed by associating polymers with multiple stickers, J. Chem. Phys. 133 (2010) 194902.
[44] M.J. Mateyisi, J.-U. Sommer, K.K. Müller-Nedebock, G. Heinrich, Influence of weak reversible cross-linkers on entangled polymer melt dynamics, J. Chem. Phys. 148 (2018) 244901.
[45] P. Xu, J. Lin, L. Wang, L. Zhang, Shear flow behaviors of rod-coil diblock copolymers in solution: a nonequilibrium dissipative particle dynamics simulation, J. Chem. Phys. 146 (2017) 184903.
[46] Y.R. Sliozberg, J.W. Andzelm, J.K. Brennan, M.R. Vanlandingham, V. Pryamitsyn, V. Ganesan, Modeling viscoelastic properties of triblock copolymers: a DPD simulation study, J. Polym. Sci., Part B: Polym. Phys. 48 (2010) 15–25.
[47] W. Hong, J. Lin, X. Tian, L. Wang, Distinct viscoelasticity of hierarchical nanostructures self-assembled from multiblock copolymers, Macromolecules 53 (2020) 10955–10963.
[48] G. Cui, V.A.H. Boudara, Q. Huang, G.P. Baeza, A.J. Wilson, O. Hassager, D.J. Read, J. Mattsson, Linear shear and nonlinear extensional rheology of unentangled supramolecular side-chain polymers, J. Rheol. 62 (2018) 1155–1174.
[49] P.J. Hoogerbrugge, J.M.V.A. Koelman, Simulating microscopic hydrodynamic phenomena with dissipative particle dynamics, Europhys. Lett. 19 (1992) 155–160.
[50] J.M.V.A. Koelman, P.J. Hoogerbrugge, Dynamic simulations of hard-sphere suspensions under steady shear, Europhys. Lett. 21 (1993) 363–368.
[51] N. Iwaoka, K. Hagita, H. Takano, Multipoint segmental repulsive potential for entangled polymer simulations with dissipative particle dynamics, J. Chem. Phys. 149 (2018) 114901.
[52] S.L. Mayo, B.D. Olafson, W.A. Goddard, DREIDING: a generic force field for molecular simulations, J. Phys. Chem. 94 (1990) 8897–8909.
[53] LAMMPS Molecular Dynamics Simulator. https://lammps.sandia.gov/. (Accessed 24 August 2021). Accessed.
[54] A. Lees, S. Edwards, The computer study of transport processes under extreme conditions, J. Phys. C Solid State Phys. 5 (1972) 1921.
[55] D.J. Evans, G.P. Morriss, Statistical Mechanics of Nonequilbrium Liquids, ANU Press, Canberra, 2007.
[56] K. Hyun, M. Wilhelm, C.O. Klein, K.S. Cho, J.G. Nam, K.H. Ahn, S.J. Lee, R. H. Ewoldt, G.H. McKinley, A review of nonlinear oscillatory shear tests: analysis and application of large amplitude oscillatory shear (Laos), Prog. Polym. Sci. 36 (2011) 1697–1753.
[57] M. Doi, S.F. Edwards, The Theory of Polymer Dynamics, Oxford University Press, Oxford, U. K., 1986.
[58] W. Hong, J. Lin, X. Tian, L. Wang, Viscoelasticity of nanosheet-filled polymer composites: three regimes in the enhancement of moduli, J. Phys. Chem. B 124 (2020) 6437–6447.
[59] M. Rubinstein, R.H. Colby, Polymer Physics, Oxford University Press, Oxford, 2003.
[60] Q. Li, L. Wang, J. Lin, Z. Xu, Distinctive morphology modifiers for polymer blends: roles of asymmetric janus nanoparticles during phase separation, J. Phys. Chem. B 124 (2020) 4619–4630.
[61] P.-G. de Gennes, Reptation of a polymer chain in the presence of fixed obstacles, J. Chem. Phys. 55 (1971) 572–579.
[62] M. Golkaram, C. Fodor, E. van Ruymbeke, K. Loos, Linear viscoelasticity of weakly hydrogen-bonded polymers near and below the sol-gel transition, Macromolecules 51 (2018) 4910–4916.
[63] M. Hayashi, A. Noro, Y. Matsushita, Viscoelastic properties of supramolecular soft materials with transient polymer network, J. Polym. Sci., Part B: Polym. Phys. 52 (2014) 755–764.